Journal of Nuclear Cardiology (2025) 45, 102180

STATE OF THE ART REVIEW

Quantitative approaches to ^{18}F-flurpiridaz positron emission tomography image analysis

René R. Sevag Packard [1,*], Robert A. deKemp [2], Juhani Knuuti [3], Jonathan B. Moody [4], Jennifer M. Renaud [4], Antti Saraste [5], Piotr J. Slomka [6]

[1] Division of Cardiology, Department of Medicine, David Geffen School of Medicine, University of California, Los Angeles, CA, USA
[2] Division of Cardiology, Department of Medicine, University of Ottawa Heart Institute, Ottawa, ON, Canada
[3] Turku PET Centre, University of Turku, and Turku University Hospital, Turku, Finland
[4] INVIA, LLC, Ann Arbor, MI, USA
[5] Heart Center, University of Turku and Turku University Hospital, Turku, Finland
[6] Cedars-Sinai Medical Center, Los Angeles, CA, USA

* Corresponding author.
E-mail address: rpackard@mednet.ucla.edu (René R. Sevag Packard).

Keywords: ^{18}F-flurpiridaz, Positron emission tomography, Myocardial perfusion imaging, Myocardial blood flow, Method, Quantitation

Key points

- ^{18}F-flurpiridaz is a positron emission tomography (PET) radiotracer for myocardial perfusion imaging (MPI) approved by the United States Food and Drug Administration in September 2024.
- This radiotracer's properties, including a very high 94% myocardial first-pass extraction fraction and positron range of 1 mm, render this probe suitable for high-resolution MPI and quantitative myocardial blood flow (MBF) determination.
- We present ^{18}F-flurpiridaz in the context of other PET MPI radiopharmaceuticals, discuss pivotal experimental studies that provided the foundation for subsequent software-based quantitative strategies in humans, and detail the published methods of relative MPI as well as MBF quantitation.
- The reviewed methods provide a standardization of ^{18}F-flurpiridaz PET and MBF interpretation that are poised to facilitate this radiotracer's adoption and implementation in cardiac imaging centers.

INTRODUCTION

Myocardial perfusion imaging (MPI) plays a crucial role in evaluating the hemodynamic significance of stenotic epicardial lesions and stratifying risk in patients with stable coronary artery disease (CAD). While positron emission tomography (PET) has demonstrated superior accuracy over single-photon emission computed tomography (SPECT) MPI, particularly in female and obese patients, and offers lower radiation exposure, its widespread adoption has been limited by logistical constraints associated with current radiopharmaceuticals.

Beyond relative perfusion imaging, which relies on the region of highest radiotracer uptake as a

Received 23 January 2025; Accepted 6 March 2025; Available online 28 March 2025

https://doi.org/10.1016/j.nuclcard.2025.102180

"normal" reference to determine epicardial CAD, absolute myocardial blood flow (MBF) quantification offers a more nuanced evaluation. Indeed, absolute MBF measurement enables clinicians to assess not only obstructive epicardial disease but also critically coronary microvascular function which can be impaired independent of major vessel stenosis. In addition, MBF quantification captures hemodynamic alterations that might be overlooked by traditional relative perfusion imaging techniques, particularly in multivessel disease [1–5], and provides a more granular patient risk stratification [6–8].

Flurpiridaz (Flyrcado), a novel ^{18}F-based PET radiopharmaceutical with a 110-min half-life, has undergone extensive phase I-III multicenter clinical investigation [9–14] and was approved for clinical use by the US Food and Drug Administration in September 2024. This tracer can be distributed to imaging centers as unit doses and is expected to significantly expand access to PET MPI.

Quantitative methods in nuclear imaging provide objective, reproducible assessments of myocardial perfusion, overcoming limitations of visual interpretation and enhancing overall diagnostic accuracy. These techniques, including automated relative perfusion scoring and absolute MBF quantification that permit standardized evaluations, have been further developed for ^{18}F-flurpiridaz PET imaging. In this review, we discuss ^{18}F-flurpiridaz in the context of other PET MPI radiotracers, highlight experimental work that provided the foundation for subsequent software-based quantitative strategies in humans, detail the published methods of relative perfusion as well as MBF quantitation, and address limitations and areas requiring further research with this radiotracer.

DIFFERENCES IN RADIOTRACERS FOR PET MPI AND MBF DETERMINATION

Characteristics of the commonly available myocardial perfusion tracers are summarized in Table 1 [15,16]. One of the important features of an ideal perfusion tracer is a linear relationship of the tracer uptake as a function of MBF [15]. The most widely available tracers have suboptimal first-pass extraction and/or retention at high flow rates; and consequently, nonlinear MBF-uptake relationships, underestimating the true MBF at higher flow rates. Therefore, a flow-dependent correction factor is needed for mathematical modeling of high-flow-range MBF. Nonetheless, large correction factors augment the noise of measurement, increasing the scatter of perfusion values at high-flow-range MBF.

• ^{82}Rubidium

^{82}Rubidium (^{82}Rb) is a potassium analog that is actively taken up by the myocardium through the membrane Na^+-K^+-Adenosinetriphosphatase

Table 1. Commonly used radionuclide tracers for myocardial perfusion imaging with positron emission tomography.

Property	^{82}Rubidium	^{13}N-ammonia	^{15}O-water	^{18}F-flurpiridaz
Physical half-life (minutes)	1.25	9.96	2.06	110
FWHM positron range (millimeter)	8.6	2.53	4.14	1.03
Production equipment	Generator	Onsite/nearby cyclotron	Onsite cyclotron	Regional cyclotron
Extraction fraction	65%	90%	100%	94%
Rest + vasodilator stress injected activity (mCi)	20 + 20	10 + 10	10 + 10	3 + 6[a]
Total rest + vasodilator stress effective dose (mSv)	1.6	1.5	.75	6.3
Effective dose constant (mSv/GBq)[b]	1.1	2.0	1.1	19
Image resolution	Good	Very good	Good	Excellent
Spillover from adjacent organs	Stomach wall	Liver and lungs	Liver	Liver
Patient examination time (min)	30	30-60	30	45-110
Vasodilator stress imaging protocol	Feasible	Feasible	Feasible	Feasible
Treadmill exercise imaging protocol	Not feasible	Feasible/not practical	Not feasible	Feasible
Approval state	FDA-approved	FDA-approved	Not FDA-approved[c]	FDA-approved

FDA, United States Food and Drug Administration; *FWHM*, full width at half maximum [16,53,54].
Typical injected doses are presented but will vary depending on the use of weight-based or high-low dosing protocols.
[a] ^{18}F-flurpiridaz 2:1 (or 3:1) dosing is recommended for vasodilator (or exercise) stress-rest imaging (Flyrcado package insert, 2024). For exercise stress, a dose of 9 mCi was used in the clinical trials [12,14].
[b] Most recent published values used for ^{82}Rubidium (ICRP128, 2015), ^{13}N-ammonia (ICRP80, 1998), ^{15}O-water (ICRP53 addendum 6, 2004), and ^{18}F-flurpiridaz (Maddahi et al. J Nucl Card, 2019 [11]).
[c] Clinically used in select European centers; a clinical trial in the US is ongoing with a 10-mCi standard dosing.

[16,17]. The physical half-life of ^{82}Rb is short, and it can be produced from local ^{82}Sr/^{82}Rb generators lasting 4-8 weeks. Since it does not need an onsite cyclotron, it is the most widely used tracer for PET MPI and MBF determination but requires high patient throughput for cost-effectiveness. Only pharmacological stress can be used with a protocol using ^{82}Rb PET MPI. On the other hand, the short half-life of ^{82}Rb enables rapid rest-stress imaging protocols. The longest positron range of ^{82}Rb among the perfusion tracers hampers image spatial resolution. The effective radiation dose is low. Theoretically, the suboptimal and nonlinear extraction fraction of ^{82}Rb makes it far from an ideal tracer for MBF quantification; however, evidence supports the feasibility, accuracy, and reproducibility of ^{82}Rb PET MPI and MBF quantitation [18–20].

- **^{13}N-Ammonia**

^{13}N-ammonia enters the myocardium by passive free diffusion across the sarcolemma, where it equilibrates with cytoplasmic ammonium and gets trapped in the cytoplasm through metabolic conversion [17,21]. The half-life of ^{13}N-ammonia (almost 10 minutes) allows for its production in a nearby cyclotron. Physical exercise testing with ^{13}N-ammonia PET MPI is impractical for routine clinical implementation. The relatively short positron range of ^{13}N-ammonia provides good spatial resolution. The extraction fraction of ^{13}N-ammonia is high, but flow-dependent correction may be used in the high-flow-range MBF, depending on the underlying compartmental model [22,23].

- **^{15}O-Water**

Being metabolically inert and freely diffusible, ^{15}O-water enters the myocardium by passive diffusion, and since it does not accumulate in the myocardium, both wash-in and wash-out are applied for absolute MBF quantification, and parametric images are used for interpretation [24–26]. Due to its short half-life, it needs an onsite cyclotron for its production, and only pharmacological stress is feasible. Similar to ^{82}Rb, ^{15}O-water enables fast rest-stress imaging protocols. A stress-only imaging protocol appears to be sufficient for most patients without previous myocardial infarction [27]. ^{15}O-water has an excellent first-pass extraction fraction that is independent of flow rate, and correction is not required [24] and provides robust MBF quantification [7,8,28].

- **^{18}F-flurpiridaz**

^{18}F-flurpiridaz PET has emerged as a promising radiotracer for MPI and MBF determination. Several phase II and phase III clinical trials demonstrated its robust diagnostic performance, including in women, obese individuals, and patients with smaller hearts [10,12–14]. ^{18}F-flurpiridaz PET offers high-quality images and enhanced diagnostic certainty [9,11]. The short positron range of ^{18}F provides the highest spatial resolution of all PET MPI radiotracers [29]. The tracer's longer half-life (~110 minutes) facilitates broader clinical access and flexibility in imaging protocols that include routine treadmill exercise stress testing [29] and further allows for unit-dose delivery from a regional cyclotron, obviating the need for an onsite cyclotron or generator. As per regulatory requirements, the reference standard for the clinical trials assessing ^{18}F-flurpiridaz relative perfusion imaging was invasive coronary angiography with a significance threshold of ≥50% stenosis.

The clinical trial ^{18}F-flurpiridaz doses were prespecified as 2.5 to 3.0 mCi for rest imaging; 6.0 to 6.5 mCi for pharmacological stress imaging, with a minimum 30-min interval between rest and stress doses; and 9.0 to 9.5 mCi for exercise stress imaging, with a minimum 1-h interval between rest and exercise doses [12,14]. For absolute MBF quantitation, residual activity correction (RAC), i.e., subtraction of the residual activity from the rest ^{18}F-flurpiridaz scan, needs to be applied prior to the stress scan [30,31]. The pharmacological and exercise stress protocols of ^{18}F-flurpiridaz derived from the phase III clinical trials are presented (Figure 1).

To date, there have not been any studies that have validated quantitation of MBF using ^{18}F-flurpiridaz in humans against a reference standard beyond % coronary stenosis, e.g., invasive coronary flow quantification by Doppler wire or thermodilution or fractional flow reserve.

PRECLINICAL EVALUATION OF ^{18}F-FLURPIRIDAZ: INSIGHTS FROM ANIMAL STUDIES

An ^{18}F-labeled tracer, ^{18}F-flurpiridaz binds to mitochondrial complex 1 of the respiratory chain (Figure 2) [32]. Initial preclinical evaluation of ^{18}F-flurpiridaz, previously called BMS-747158, demonstrated favorable characteristics for MPI, including very high and sustained myocardial uptake proportional to MBF, and high contrast between the myocardium and adjacent organs [32–37].

^{18}F-flurpiridaz PET images showed clear visualization of the left ventricular (LV) myocardium with a high target-to-background ratio in all tested

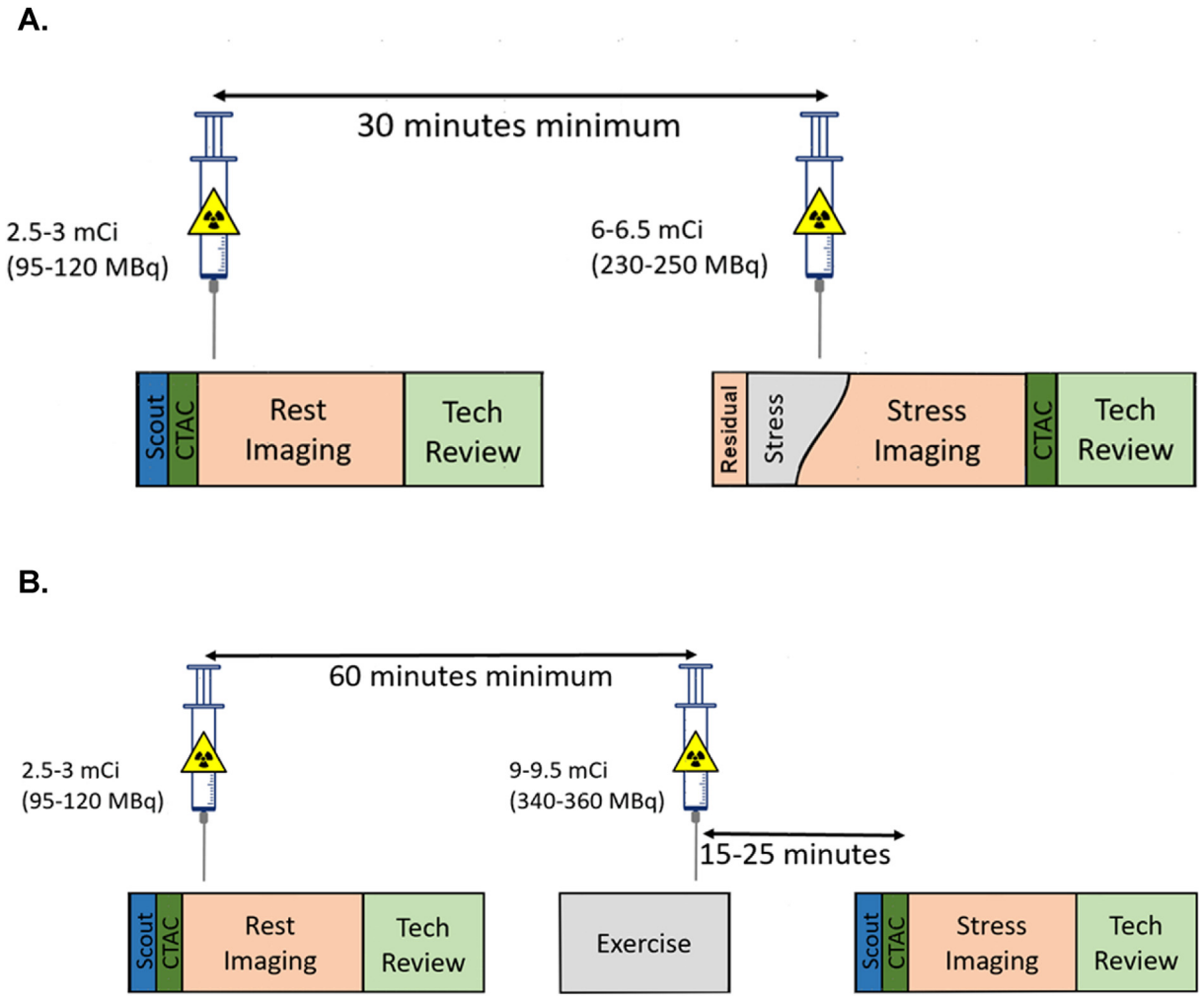

Figure 1. ^{18}F-Flurpiridaz protocols for pharmacological (A) and exercise (B) stress imaging. Residual frame(s) of sufficient duration should be acquired before pharmacological stress injection for residual activity correction. Pharmacological stress with regadenoson, adenosine, or dipyridamole should be conducted according to the manufacturer's instruction. Images adapted from GE HealthCare with substantial modifications. These protocols are anticipated to evolve with clinical usage of ^{18}F-flurpiridaz. *CTAC, computed tomography-based attenuation correction.*

species, including rats, rabbits, pigs, and nonhuman primates [33–36]. In a normal pig heart, distribution of radioactivity was homogeneous, similar to that of ^{13}N-ammonia [35]. Image-derived activity ratios between the myocardium and blood, liver, and lungs were approximately 2 to 3 times higher with ^{18}F-flurpiridaz compared to ^{13}N-ammonia at rest and during pharmacological stress [35]. ^{18}F-flurpiridaz PET images also showed clear delineation of regional perfusion defects during pharmacological stress, induced by acute constriction of the left anterior descending artery [35]. In rats, the extent of ^{18}F-flurpiridaz defects showed a good correlation and agreement with histologically determined myocardial infarct size after permanent ($r = .88$, $\Delta = 1.9\%$) or transient ($r = .92$, $\Delta = 2.2\%$) coronary artery occlusion [36].

Several preclinical studies investigated the properties of ^{18}F-flurpiridaz extraction and retention that were critical to support the tracer's potential for MBF quantification. Myocardial first-pass extraction (E_0) of ^{18}F-flurpiridaz has been studied after a bolus injection in isolated rat hearts perfused with increasing flow rates, demonstrating a high and flow-independent myocardial first-pass extraction fraction averaging 94% over a wide range of whole-heart flow rates [34]. Similarly, in isolated rabbit hearts, myocardial uptake of ^{18}F-flurpiridaz increased proportionally to flows of up to 5 mL/min/g of LV weight [33]. With increasing flows, the uptake of ^{18}F-flurpiridaz increased to a greater extent than that of ^{201}Tl or ^{99m}Tc-sestamibi [33].

Validation studies in pigs demonstrated the feasibility and accuracy of MBF quantification with ^{18}F-flurpiridaz PET using a 2-tissue compartment model without corrections for metabolites or flow-dependent extraction [35,38,39].

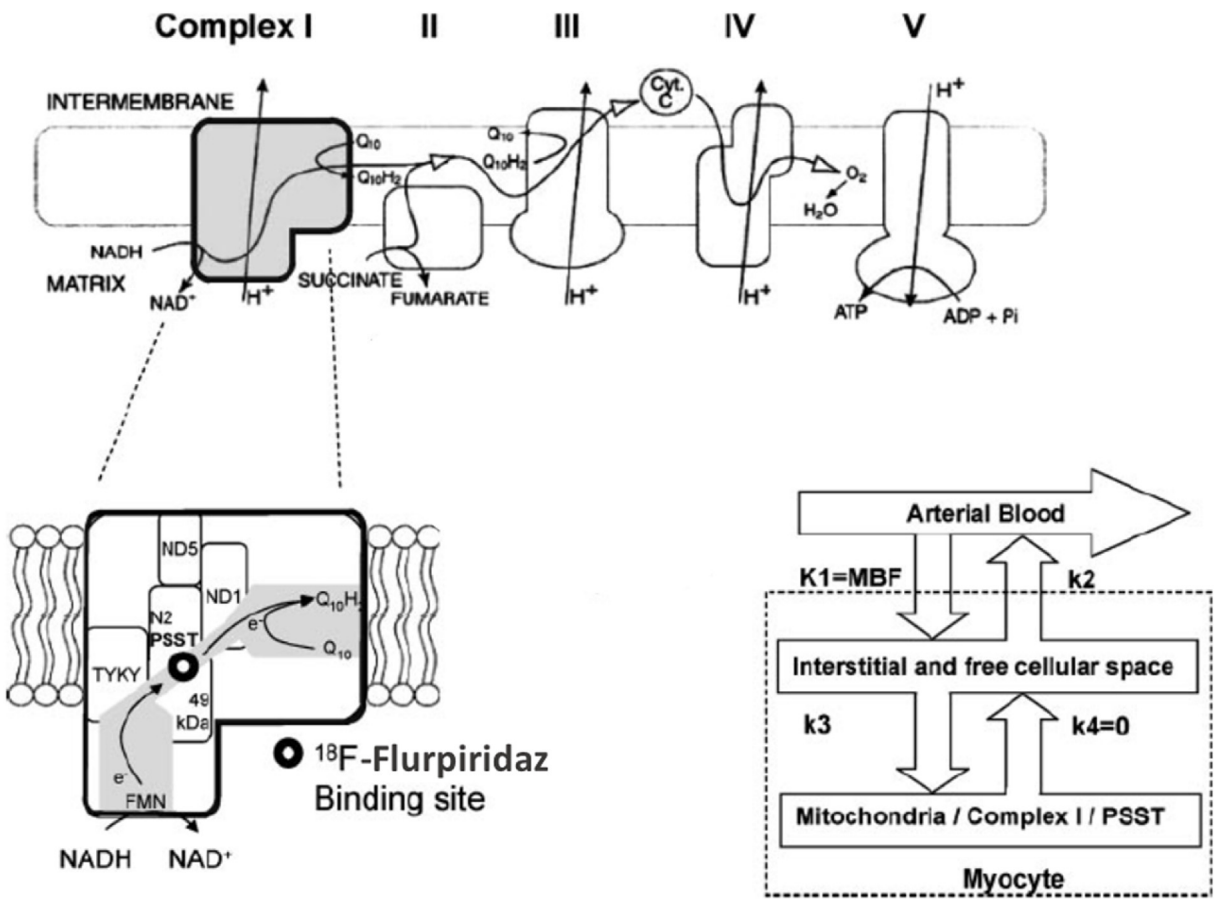

Figure 2. **Biological mechanism of ^{18}F-flurpiridaz retention.** The biological mechanism of ^{18}F-flurpiridaz retention is irreversible binding to the PSST subunit (also known as 20 kD subunit) (bottom left) of mitochondrial Complex I (NADH:ubiquinone oxidoreductase) in the electron transport chain (top). A two-tissue compartment model (bottom right) was used for validation of the transport rate-constant K_1 against microspheres-standard myocardial blood flow (MBF) in pigs. PSST and TYKY are two important subunits of mitochondrial complex I. Figure adapted from Ref. [35].

In vivo measurements of the blood-to-tissue transport rate constant K_1 provided accurate estimates of MBF in regions of normal myocardium at rest and during pharmacological stress [35]. Regional MBF showed a good correlation with that measured using microspheres ($r = .88$, $\Delta = -.10$ mL/g/min) over a wide flow range from .1 to 3.0 mL/min/g achieved using a combination of pharmacologic stress and epicardial coronary artery constriction [35].

RELATIVE ^{18}F-FLURPIRIDAZ PET MYOCARDIAL PERFUSION QUANTITATION

While visual assessment of relative perfusion based on radiotracer count distribution in regional myocardial tissue remains the primary method of MPI interpretation, automated approaches have been developed for both SPECT and PET that standardize interpretation and reduce variability. These quantitative parameters of cardiac radionuclide distribution assist interpreting physicians in their analysis. To quantify relative perfusion, the patient's myocardial perfusion polar map is normalized to the region with the highest tracer uptake and then compared to a normal perfusion distribution database consisting of patients with normal studies acquired using a similar protocol and the same tracer, allowing for assessment of defect extent and severity. The most commonly used metrics are summed segmental scores and total perfusion deficit (TPD). For these metrics, normal database thresholds are mapped to severity scores, automatically deriving severity polar maps and 17-segment regional scoring maps for stress and rest studies. TPD is a combined measure of defect extent and severity that is a higher resolution metric than segmental scoring since it is derived at the polar map sector level [40,41].

An automated method for relative quantitation of ^{18}F-flurpiridaz PET MPI was developed [42] using data derived from the 1st phase III clinical trial evaluating this radiotracer [12]. A reference group ($n = 40$) was first used to establish a baseline ^{18}F-flurpiridaz count distribution in coronary territories and global LV myocardium, which was

then used to establish critical thresholds for MPI interpretation in a separate derivation cohort (n = 90). Specifically, the lower limits of normal radiotracer distribution and cut-off value thresholds indicative of significant CAD were determined, calibrated to detect both moderate (≥50%) and severe (≥70%) coronary stenosis. For both pharmacological and exercise stress, the optimal threshold was ≥8% LV myocardium displaying abnormal counts for CAD ≥50% stenosis and ≥12% of the LV myocardium for CAD ≥70%. The aforementioned criteria for abnormality were true both for global CAD and individual territory CAD detection. Finally, the method was validated using a separate large cohort (n = 548). The reference standard was blinded quantitative invasive coronary angiography conducted by a core laboratory for the clinical trial [12]. The automated perfusion quantification method demonstrated a diagnostic accuracy comparable to that of blinded visual interpretation (Figure 3) while achieving significantly higher interobserver agreement in both pharmacological and exercise stress studies.

An earlier study evaluated a subset of patients from the 1st phase III ^{18}F-flurpiridaz clinical trial [12] with high-quality pharmacological stress studies (n = 231) [43]. For each patient dataset, a myocardial perfusion polar map was generated from the maximum activity sampled between the LV endocardial and epicardial surfaces. Polar maps were normalized to the highest-intensity region [44] and compared to a tracer-specific normal database (n = 32) to determine stress TPD. Multivariable logistic regression models of (i) standard clinical variables (age, sex, body mass index, and pretest likelihood of CAD) alone (base model) and (ii) with the addition of stress TPD were tested for detection of ≥70% stenosis, using blinded quantitative invasive coronary angiography as the reference standard. Stress TPD was found to be a significant independent predictor of obstructive disease and to have incremental value over standard clinical covariates at both the per-vessel and per-patient levels (Figure 4) with similar results observed for detection of ≥50% stenosis. These results elucidate the utility of quantitative perfusion for detection of disease in ^{18}F-flurpiridaz PET MPI studies.

The high resolution of ^{18}F-flurpiridaz allows to enhance the visualization of the myocardium with advanced correction for cardiac and respiratory motion [45]. Such dual (respiratory/cardiac)-gated perfusion imaging with ^{18}F-flurpiridaz is feasible and improves image resolution, contrast, and contrast-to-noise ratio. The contrast-to-noise ratio almost doubles from 22.2 ± 9.1 with ungated perfusion studies to 42.1 ± 13.2 with dual cardiorespiratory gated images. An example of cardiac, respiratory, and dual corrections of ^{18}F-flurpiridaz perfusion images is shown (Figure 5).

These automated quantitation methods for ^{18}F-flurpiridaz PET MPI represent a significant step forward in standardizing interpretation and are poised to facilitate its adoption and implementation in cardiac imaging centers.

MYOCARDIAL BLOOD FLOW QUANTITATION BY ^{18}F-FLURPIRIDAZ PET

Quantification of MBF with ^{18}F-flurpiridaz is based on the principles of radiolabeled tracer exchange that are well established for other retained perfusion tracers such as ^{13}N-ammonia and ^{82}Rubidium (Table 2). The biological mechanism of ^{18}F-flurpiridaz retention within cardiomyocytes is illustrated in Figure 2.

Quantification of MBF in humans was first reported by Packard et al. [46], demonstrating the ability to stratify those with vs. without obstructive defined as CAD ≥50%. Subsequently, MBF has been investigated mainly in patients who were part of the 1st phase III clinical trial (NCT01347710) [12]. Moody et al. [43] demonstrated that ^{18}F-flurpiridaz MBF metrics provide incremental diagnostic values over relative MPI (Figure 4). A progressive reduction in stress MBF and myocardial flow reserve (MFR) in patients with increasing risk factors and in those with increased severity of disease was also observed [43].

Taking advantage of the 1 mm positron range of ^{18}F (Table 1), Packard et al. [47] established the feasibility, precision, and improved diagnostic performance of segmental over traditional coronary territory MBF measurements using ^{18}F-flurpiridaz PET (Figure 6). Segmental flow metrics, defined as the lowest 17-segment stress MBF, MFR), or relative flow reserve value for each coronary territory, showed superior diagnostic performance compared to their territory counterparts [47]. This improvement in diagnostic accuracy was consistent across per-vessel and per-patient analyses in both moderate (≥50% stenosis) and severe (≥70% stenosis) CAD.

Otaki et al. [30] demonstrated that the diagnostic performance of ^{18}F-flurpiridaz PET stress MBF and MFR significantly improved through the implementation of RAC, manual frame-by-frame motion correction, and minimal segmental quantification in dynamic PET. These techniques proved crucial in enhancing the accuracy of MBF estimation using ^{18}F-flurpiridaz PET (Figure 7) [30]. Similar results were recently demonstrated with the use of fully automatic motion correction

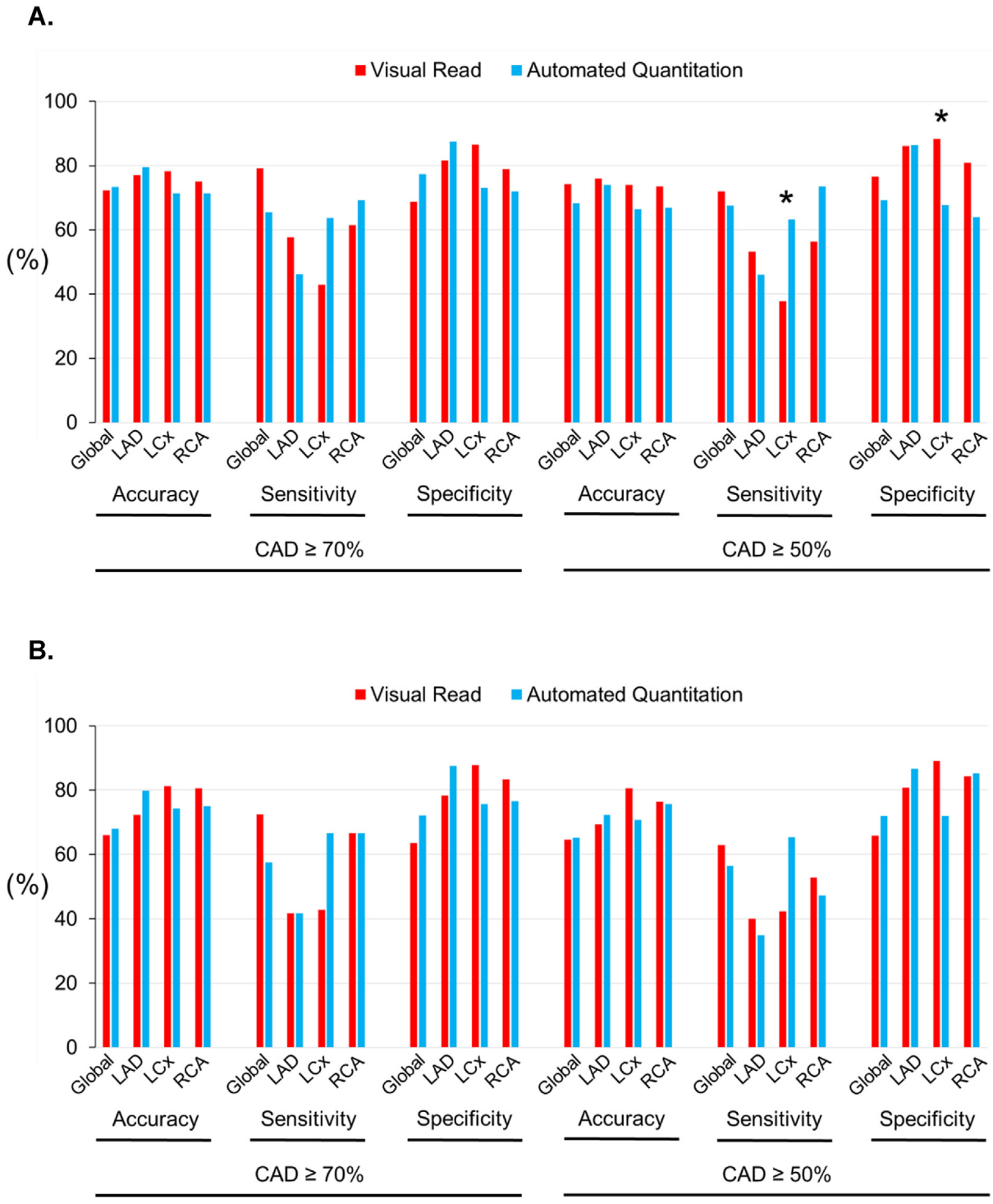

Figure 3. Diagnostic accuracy of ^{18}F-flurpiridaz automated relative perfusion quantification compared to visual reads in pharmacological (A) and exercise (B) stress. Comparison of performance metrics with the reference standard of angiographically determined CAD. *$P < .05$. Figure adapted from Ref. [42]. *CAD, coronary artery disease; LAD, left anterior descending artery; LCx, left circumflex artery; RCA, right coronary artery.*

algorithm by Builoff et al. [48] (Figure 8), confirming the need for routine correction of dynamic interframe motion in the clinical MBF studies. Clinical cases illustrating the impact of motion correction (Figure 9) and residual activity correction (Figure 10) on ^{18}F-flurpiridaz MBF and MFR values are presented.

The need for rest RAC is paramount in same-day protocols as the brief interval between rest and stress injections relative to the 110-min half-life of ^{18}F results in significant residual activity from the rest injection persisting in the myocardium during stress imaging, necessitating adjustment to ensure accurate MBF

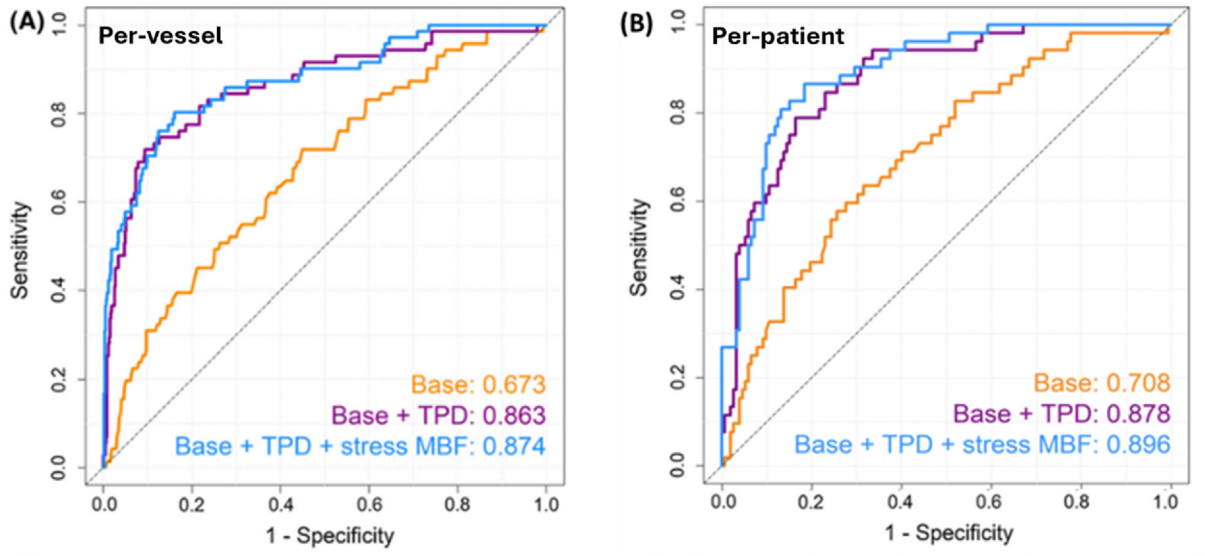

	Base	Base + TPD	Base + TPD + stress MBF
χ^2	19.0	110.8	153.3
p-value	–	<0.0001	<0.0001

	Base	Base + TPD	Base + TPD + stress MBF
χ^2	21.3	77.7	91.9
p-value	–	<0.0001	0.0002

Figure 4. Incremental value of ^{18}F-flurpiridaz MPI and MBF over clinical variables. ROC curves of (A) per-vessel and (B) per-patient CAD diagnosis (70% stenosis threshold) derived from multivariable logistic regression models. In both cases, stress total perfusion deficit (TPD) added significant incremental value to the Base model, and likewise stress MBF added significant incremental value to the Base + stress TPD model. The Base model included patient age, sex, body mass index, and pre-test likelihood of CAD. Figure legends indicate c-index values for each nested model. Figure adapted from Ref. [43]. *CAD*, coronary artery disease; *MBF*, myocardial blood flow; *MPI, myocardial perfusion imaging; TPD, total perfusion deficit.*

quantification [30]. The residual rest activity can be measured at the start of the stress scan (before ^{18}F-flurpiridaz injection) and subtracted from the dynamic image data before MBF estimation, as proposed originally by Nekolla et al. [35]. This method has been adopted by all the ^{18}F-flurpiridaz MBF software methods as reported in recent clinical studies [30,31,43,47]. An alternative approach was proposed in the study by Guehl et al. [39], where the rest and stress data are acquired in one continuous scan followed by simultaneous estimation of rest and stress MBF values from the corresponding imaging intervals.

Sherif et al. [38] introduced a simplified, model-free approach to estimate MBF and MFR using standardized uptake values (SUVs) measured 5-10 minutes after ^{18}F-flurpiridaz injection. They demonstrated a linear correlation between SUV and MBF measured with microspheres at rest and during pharmacologic stress, while the SUV ratio between stress and rest provided a reliable estimate of MFR. This approach eliminates the need for kinetic modeling, which would make it particularly valuable for patients undergoing treadmill exercise ^{18}F-flurpiridaz PET, where current time-activity curve–based methods prevent MBF determination. While this method holds promise for broad clinical application, its demonstration in patients is pending.

CURRENT LIMITATIONS

Further human studies are necessary to validate ^{18}F-flurpiridaz MBF accuracy against an established PET myocardial perfusion tracer, as well as to determine MBF test-retest repeatability. Although extensive studies have been performed in various animal models as outlined earlier, several questions pertinent to perfusion quantification in humans remain. Some limited data suggest that tracer binding to blood components and metabolism on a time scale relevant for MBF measurement may affect the accuracy of the arterial input function. Measurements in rats showed rapid tracer metabolism (parent fraction 40% at 5 minutes, and 24% at 10 minutes post injection) and approximately constant plasma-to-whole blood ratio (PWR ~1.28 over 60 minutes post injection) [49]. In pigs, Guehl et al. [39] applied tracer blood-binding measurements to correct the arterial input function and found good MBF correlation with microsphere reference measurements. Nekolla et al. [35], also studying ^{18}F-flurpiridaz in pigs, did not apply blood-

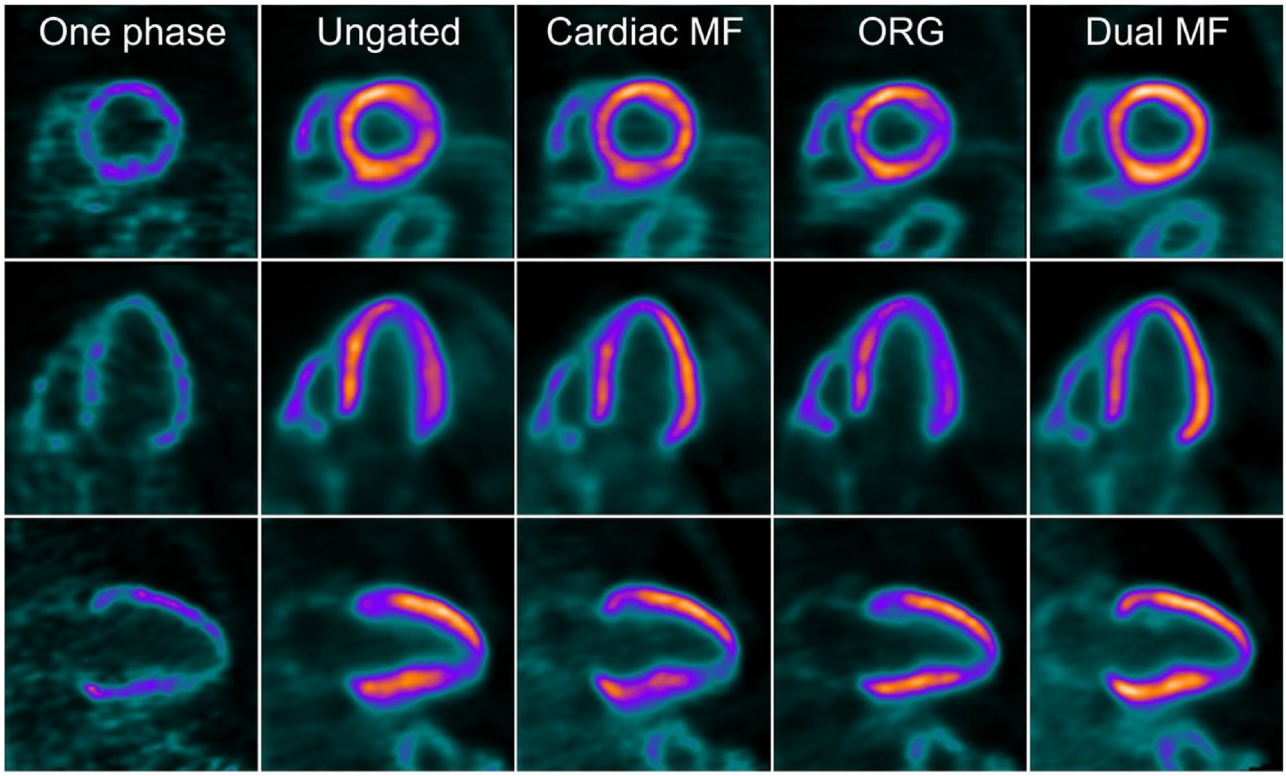

Figure 5. Dual-gated, motion-frozen ^{18}F-flurpiridaz PET MPI. A 67-year-old male patient with prior myocardial infarction (weight: 88.5 kg [195 lbs]; body mass index: 25.7 kg/m^2) injected with 355.2 MBq (9.6 mCi) of ^{18}F-flurpiridaz during adenosine stress and acquired in dual (cardiac and respiratory) motion frozen mode. Short-, horizontal-, and vertical-axis views of adenosine stress images. One phase = 1 cardiac gate in end-inspiration; cardiac MF = cardiac MF with no respiratory gating; ORG = optimal respiratory gating with no cardiac gating; dual MF = dual (cardiac + respiratory) MF. Figure reproduced from Ref. [45]. *MF, motion frozen; MPI, myocardial perfusion imaging; PET, positron emission tomography.*

Table 2. Per-patient diagnostic performance of ^{18}F-flurpiridaz myocardial blood flow metrics vs. invasive coronary angiography.

Study (topic)	Population	Stress protocol (flow model)	Parameters	AUC	
				CAD: ≥50	CAD: ≥70
Packard 2014 (lesion stratification)	Healthy controls (n = 7) CAD patients (n = 8)	Adenosine (1.5 min retention)	Stress MBF MFR	NA	NA
Moody 2020 (incremental value vs MPI)	Phase 3-301 trial CAD patients (n = 231)[a]	Pharmacologic (15 min 2TCM)	Stress MBF MFR	.79 .71	.83 .79
Packard 2022 (segmental minimum)	Phase 3-301 trial CAD patients (n = 245)[a]	Pharmacologic stress (4 min retention)	Stress MBF MFR	.77 .71	.82 .79
Poitrasson-riviere 2022 (RAC)	Phase 3-301 trial CAD patients (n = 231)[a]	Pharmacologic (15 min 2TCM)	Stress MBF MFR	NA	.83 .78
Otaki 2022 (RAC and MoCo)	Phase 3-301 trial CAD patients (n = 231)[a]	Pharmacologic (2 min retention)	Stress MBF MFR	NA	.89 .87
Choueiry 2023 (exercise MFR)	Phase 3-301 trial CAD patients (n = 120)	Exercise (SUVR)	MFR	.73	.80
Builoff 2024 (manual vs auto MoCo)	Phase 3-301 trial CAD patients (n = 231)[a]	Pharmacologic (2 min retention)	Stress MBF MFR	NA	.89 .87

2TCM, Two-tissue compartment model; *AUC*, area under the curve; *CAD*, coronary artery disease; *MBF*, myocardial blood flow. *MFR*, myocardial flow reserve; *MoCo*, motion correction; *MPI*, myocardial perfusion imaging; *RAC*, residual activity correction; *SUVR*, standard uptake value ratio; *NA*, not available. Pharmacologic stress indicates regadenoson, adenosine, or dipyridamole.
[a] Subset of the phase 3-301 trial patients with analyzable dynamic rest and pharmacologic stress images.

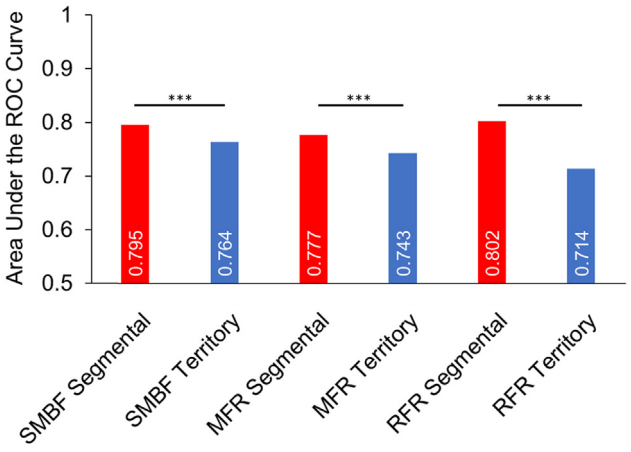

Figure 6. Per-vessel diagnostic performance of segmental vs territory ^{18}F-flurpiridaz MBF metrics. For CAD ≥70% categorization of pooled coronary territories (n = 735), all the segmental ^{18}F-flurpiridaz flow metrics demonstrated significantly greater diagnostic performance than their territory counterparts. MFR was calculated as stress MBF divided by rest MBF. Territory RFR was defined as the ratio of stress MBF in a specific coronary territory to the highest stress MBF among all territories. Segmental flow was determined using the 17-segment American Heart Association left ventricular model. Each territory's segmental flow metric was the lowest value of rest MBF, stress MBF, or MFR. Segmental RFR was determined by dividing the lowest segmental stress MBF in a territory by the highest segmental stress MBF in the territory with maximum flow. *CAD*, coronary artery disease; *MBF*, *myocardial blood flow*; *MFR*, myocardial flow reserve; *RFR*, relative flow reserve; *ROC*, receiver operating characteristic; *SMBF*, stress myocardial blood flow. ***$P < .001$. Figure adapted from Ref. [47].

binding or metabolite corrections and observed a modest MBF underestimation compared to microspheres. In general, a PWR greater than 1.0 would lead to MBF overestimation, and uncorrected tracer metabolism would produce MBF underestimation, and thus, to some extent, the two errors could partially offset each other. However, the magnitude of these effects in humans has not yet been reported.

In practice, tracer metabolism can be mitigated by using only the first 2-4 minutes of dynamic data post injection or by applying a population-

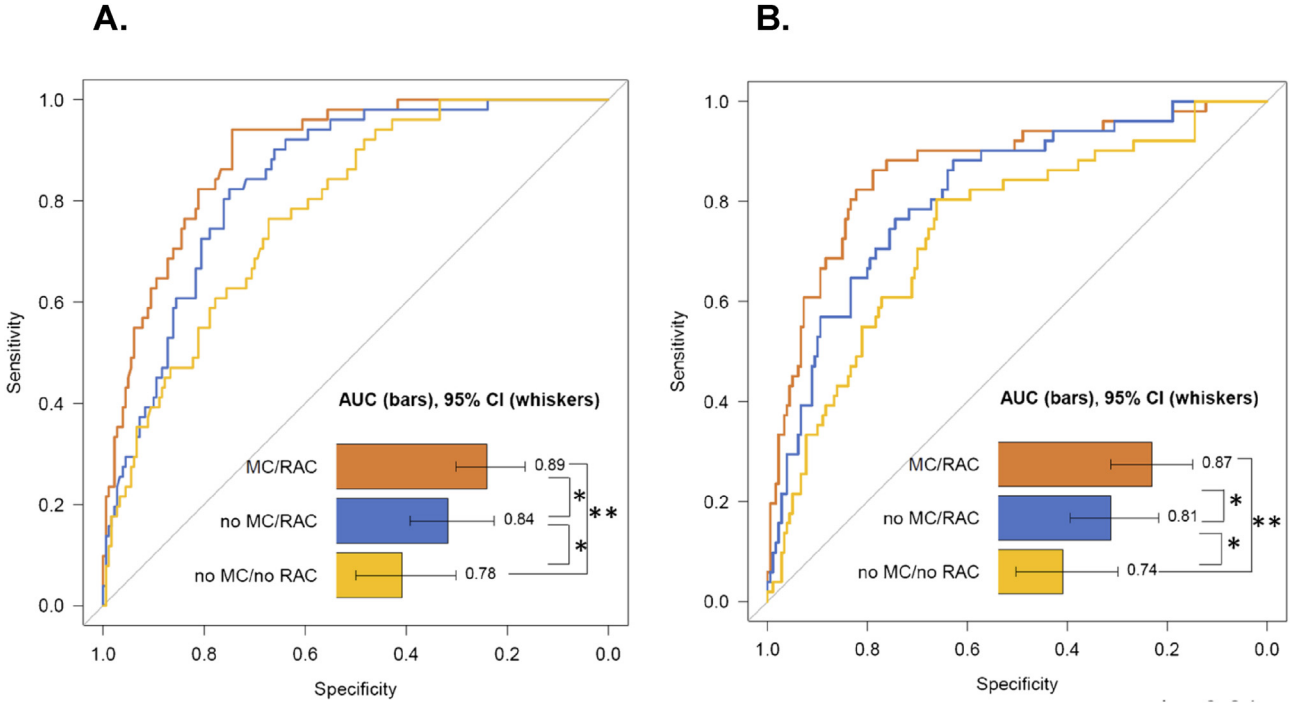

Figure 7. Motion correction and residual activity correction significantly impact the diagnostic performance of ^{18}F-flurpiridaz Stress myocardial blood flow (A) and myocardial flow reserve (B). Reference standard: ≥70% stenosis in one the three coronary arteries or ≥50% stenosis in the left main coronary artery by invasive coronary angiography. *AUC*, area under the receiver operating characteristic curve; *CI*, confidence interval; *MC*, motion correction; *RAC*, residual activity correction. *$P < .01$, **$P < .0001$. Figure reproduced from Ref. [30].

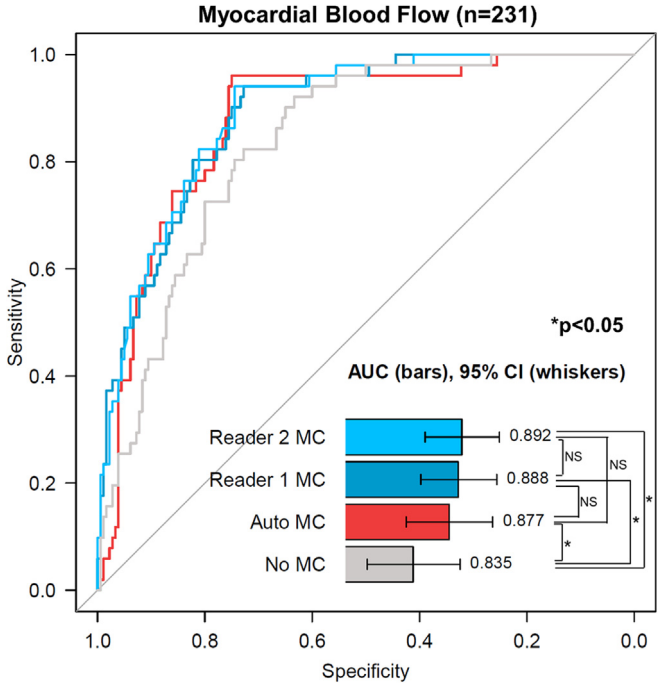

Figure 8. Automatic motion correction for ^{18}F-flurpiridaz myocardial blood flow (MBF) determination. Per-patient diagnostic performance of stress MBF, with residual activity correction, compared among manual motion correction (MC) from Reader 1 (medium blue), manual MC from Reader 2 (light blue), automatic (Auto) MC (red), and no MC (gray). *AUC,* area under the receiver operating characteristic curve; *CI,* confidence interval; *NS,* not significant. Figure reproduced from Ref. [48].

averaged correction to the arterial input function, as reported for ^{13}N-ammonia [50,51]. Although ^{82}Rb does not undergo metabolism, blood binding has been reported [52] which is implicitly compensated for by the empirical extraction correction [18]. For ^{18}F-flurpiridaz, the importance of these effects is currently unknown, but they may contribute to systematic errors and increased variability of MBF, negatively affecting the definition of consistent thresholds for abnormal MBF.

A further limitation is that PET protocols reported to date have not been optimized for dynamic acquisition and MBF estimation. As described earlier, residual activity present in the stress scan must be corrected but requires sufficient dynamic data before tracer infusion to accurately estimate the residual activity. In addition, manual injection of the tracer with a 10-sec/frame temporal sampling during the blood pool phase may contribute to increased variability of the arterial input function.

FUTURE DIRECTIONS

While ^{18}F-flurpiridaz has demonstrated promising diagnostic performance for relative MPI and absolute MBF quantification, several key areas require further investigation to maximize its clinical utility. Future studies should establish and validate MBF cut-offs for abnormal flow, expanding upon findings from the 1st phase III trial across diverse populations and ideally applying invasive functional reference standards. The ideal methods for postprocessing in perfusion and flow quantification remain undetermined and should be clarified in subsequent research. Gated functional analysis, particularly LV ejection fraction, has not yet been reported and warrants exploration to enhance the evaluation of cardiac function. With increased image resolution and potential respiratory correction of gated imaging, the normal thresholds for LV volumes may need to be established. Software-based methods offer advanced motion correction for oncological imaging which may also be validated for ^{18}F high-resolution imaging. Future research should involve conducting comprehensive comparative analyses of combined cardiac and respiratory motion correction across various PET and SPECT MPI radiotracers, enabling a more thorough evaluation of the relative improvements achieved with ^{18}F-flurpiridaz PET MPI than other imaging agents. Moreover, incorporating computed tomography (CT) attenuation and integrating coronary calcium with ^{18}F-flurpiridaz data in current PET/CT imaging could yield a more comprehensive diagnostic overview from the entire stress/rest scan.

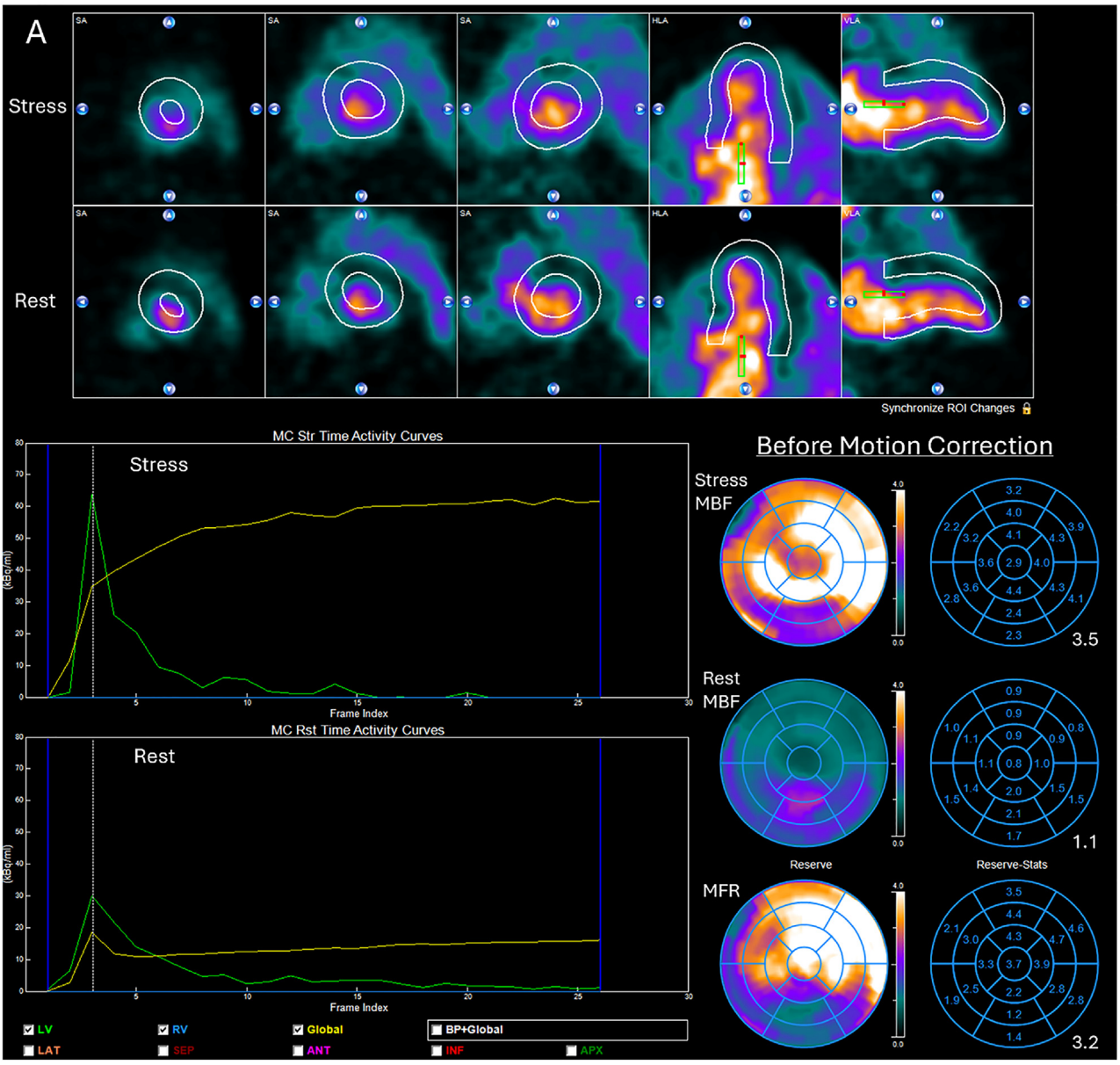

Figure 9. Case example of ^{18}F-flurpiridaz myocardial blood flow quantification (A) before and (B) after motion correction. Patient motion during the early blood pool frames, including those frames used for residual activity correction, can have a large impact on MBF and MFR estimation. Green curves: left ventricular (LV) input function. Yellow curves: global LV myocardial time-activity curves. *MBF*, myocardial blood flow; *LV*, left ventricular; *MC*, motion correction; *MFR*, myocardial flow reserve.

Furthermore, stress-only protocols, currently applied primarily to SPECT MPI, may become practical in ^{18}F-flurpiridaz PET, given the high diagnostic accuracy of stress MBF and the potential detrimental effect of rest activity on stress imaging for this tracer. These protocols could become particularly valuable if the future unit-dose cost of ^{18}F-flurpiridaz limits widespread adoption of stress/rest clinical imaging.

The impact of manual vs. automated ^{18}F-flurpiridaz injection on MBF quantification should be evaluated, as well as the potential benefits of a saline chase in ensuring consistent tracer delivery and minimizing variability.

The compartmental modeling approach for ^{18}F-flurpiridaz MBF quantification requires further validation in human studies to ensure both accuracy and reproducibility. Optimizing dynamic

B.

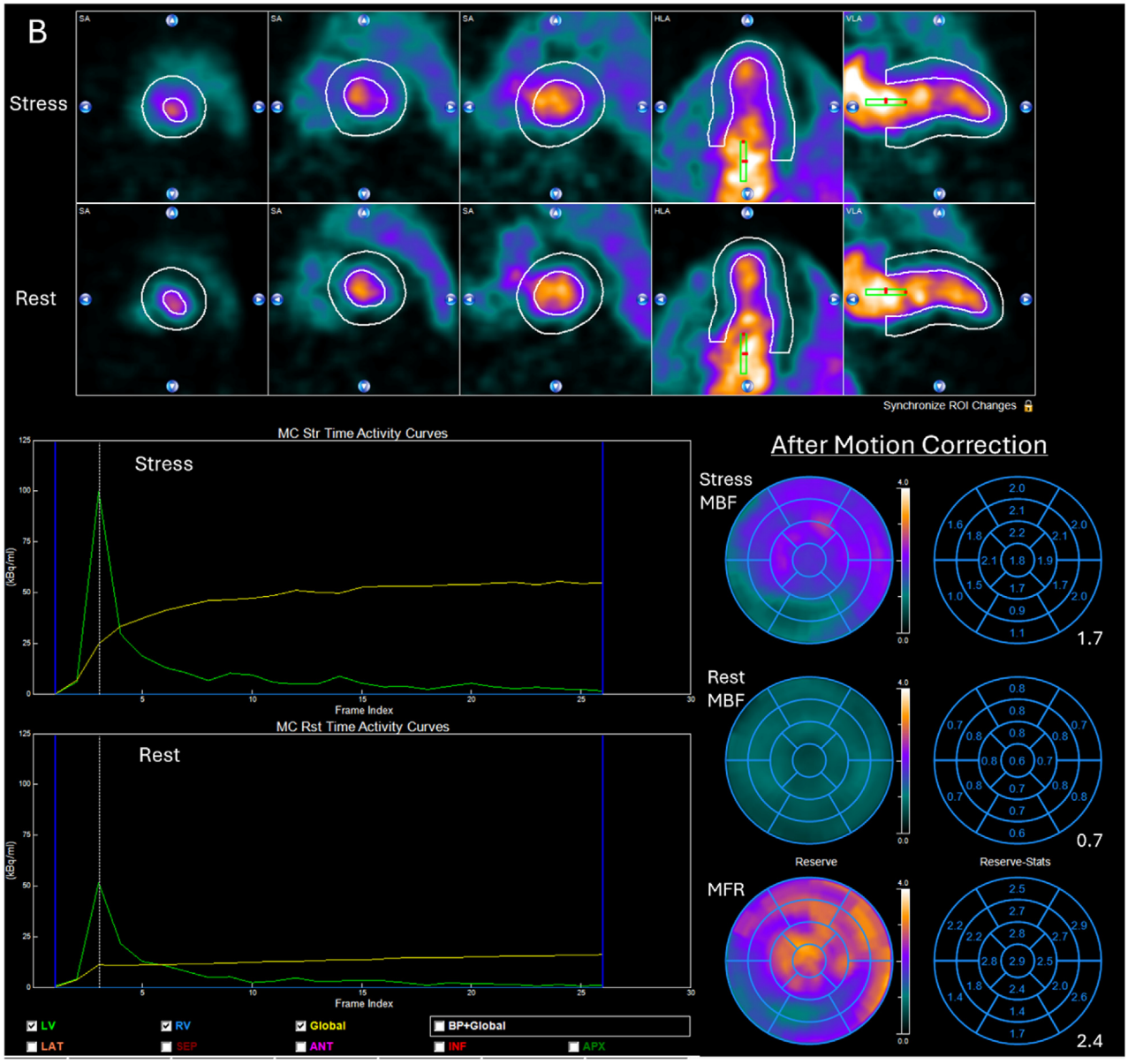

Figure 9. *(continued)*

acquisition protocols, including enhanced RAC and improved arterial input function estimation, could substantially reduce variability in MBF measurements. Simplified kinetic models and automatic quality control procedures suitable for adoption in less experienced centers will be of key importance in rolling out broad clinical utilization of ^{18}F-flurpiridaz imaging. Additionally, investigating the tracer's metabolic pathways and blood-binding characteristics is essential for identifying and addressing potential sources of error and variability in MBF quantification. Systematic assessment of test-retest repeatability for relative perfusion, MBF, and gated measures will be also crucial to establish reliability in clinical practice.

Importantly, prognostic studies linking ^{18}F-flurpiridaz MPI and MBF data to long-term outcomes are vital to evaluate its impact on clinical decision-making and patient care. Addressing these research priorities will reinforce the role of ^{18}F-flurpiridaz in advancing noninvasive cardiac imaging and ultimately improving patient outcomes.

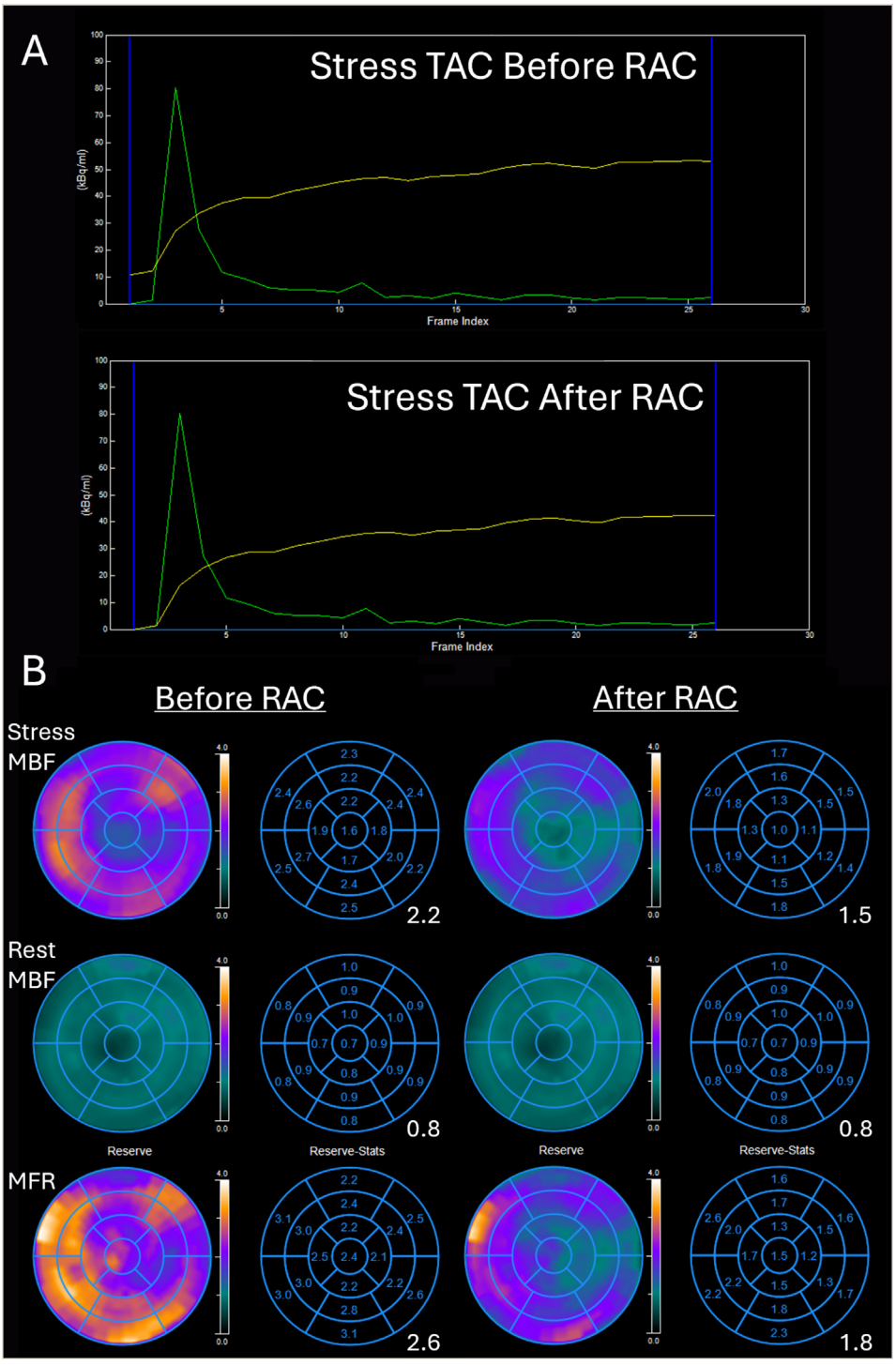

Figure 10. Case example of the impact of ^{18}F-flurpiridaz residual activity correction on stress myocardial time-activity curves (A) and global and regional stress MBF and MFR estimates (B). RAC should be systematically conducted in same-day rest/stress protocols to avoid overestimation of stress MBF and MFR values. Green curves: left ventricular (LV) input function. Yellow curves: global LV myocardial time-activity curves. *LV*, left ventricular; *MBF*, myocardial blood flow; *MFR*, myocardial flow reserve; *RAC*, residual activity correction; *TAC*, time-activity curve.

DISCLOSURES

R.R.S. Packard: consultant, GE HealthCare.

R.A. deKemp: funding, Jubilant Drax-Image Inc.; patent with royalties paid to the Ottawa Heart Institute Research Corporation.

J. Knuuti: financial support, Research Council of Finland, Finnish Foundation for Cardiovascular Research, Finnish State Research Funding, and InFlames Flagship, Finland; consultant, GE HealthCare and Synektik; speaker fees, Siemens.

J.B. Moody: salaried employee, INVIA, LLC.

J.M. Renaud: salaried employee, INVIA, LLC.

A. Saraste: financial support, Research Council of Finland, Finnish Foundation for Cardiovascular Research, Finnish State Research Funding, and InFlames Flagship, Finland; consultant, Astra Zeneca, Novo Nordisk, Pfizer; speaker fees, Abbott, Astra Zeneca, BMS, Janssen, Pfizer.

P.J. Slomka: royalties, Cedars-Sinai QPET software.

FUNDING AND SUPPORT

None.

REFERENCES

[1] Berman DS, Kang X, Slomka PJ, Gerlach J, de Yang L, Hayes SW, et al. Underestimation of extent of ischemia by gated SPECT myocardial perfusion imaging in patients with left main coronary artery disease. J Nucl Cardiol 2007;14:521–8.

[2] Knuuti J, Saraste A. Advances in clinical application of quantitative myocardial perfusion imaging. J Nucl Cardiol 2012;19:643–6.

[3] Kajander SA, Joutsiniemi E, Saraste M, Pietila M, Ukkonen H, Saraste A, et al. Clinical value of absolute quantification of myocardial perfusion with (15)O-water in coronary artery disease. Circ Cardiovasc Imaging 2011;4:678–84.

[4] Ziadi MC, Dekemp RA, Williams K, Guo A, Renaud JM, Chow BJ, et al. Does quantification of myocardial flow reserve using rubidium-82 positron emission tomography facilitate detection of multivessel coronary artery disease? J Nucl Cardiol 2012;19:670–80.

[5] Schindler TH, Quercioli A, Valenta I, Ambrosio G, Wahl RL, Dilsizian V. Quantitative assessment of myocardial blood flow–clinical and research applications. Semin Nucl Med 2014;44:274–93.

[6] Murthy VL, Naya M, Foster CR, Hainer J, Gaber M, Di Carli G, et al. Improved cardiac risk assessment with noninvasive measures of coronary flow reserve. Circulation 2011;124:2215–24.

[7] Danad I, Raijmakers PG, Driessen RS, Leipsic J, Raju R, Naoum C, et al. Comparison of coronary CT angiography, SPECT, PET, and hybrid imaging for diagnosis of ischemic heart disease determined by fractional flow reserve. JAMA Cardiol 2017;2:1100–7.

[8] Knuuti J, Ballo H, Juarez-Orozco LE, Saraste A, Kolh P, Rutjes AWS, et al. The performance of non-invasive tests to rule-in and rule-out significant coronary artery stenosis in patients with stable angina: a meta-analysis focused on post-test disease probability. Eur Heart J 2018;39:3322–30.

[9] Maddahi J, Czernin J, Lazewatsky J, Huang SC, Dahlbom M, Schelbert H, et al. Phase I, first-in-human study of BMS747158, a novel 18F-labeled tracer for myocardial perfusion PET: dosimetry, biodistribution, safety, and imaging characteristics after a single injection at rest. J Nucl Med 2011;52:1490–8.

[10] Berman DS, Maddahi J, Tamarappoo BK, Czernin J, Taillefer R, Udelson JE, et al. Phase II safety and clinical comparison with single-photon emission computed tomography myocardial perfusion imaging for detection of coronary artery disease: flurpiridaz F 18 positron emission tomography. J Am Coll Cardiol 2013;61:469–77.

[11] Maddahi J, Bengel F, Czernin J, Crane P, Dahlbom M, Schelbert H, et al. Dosimetry, biodistribution, and safety of flurpiridaz F 18 in healthy subjects undergoing rest and exercise or pharmacological stress PET myocardial perfusion imaging. J Nucl Cardiol 2019;26:2018–30.

[12] Maddahi J, Lazewatsky J, Udelson JE, Berman DS, Beanlands RSB, Heller GV, et al. Phase-III clinical trial of fluorine-18 flurpiridaz positron emission tomography for evaluation of coronary artery disease. J Am Coll Cardiol 2020;76:391–401.

[13] Packard RRS, Lazewatsky JL, Orlandi C, Maddahi J. Diagnostic performance of PET versus SPECT myocardial perfusion imaging in patients with smaller left ventricles: a substudy of the (18)F-flurpiridaz phase III clinical trial. J Nucl Med 2021;62:849–54.

[14] Maddahi J, Agostini D, Bateman TM, Bax JJ, Beanlands RSB, Berman DS, et al. Flurpiridaz F-18 PET myocardial perfusion imaging in patients with suspected coronary artery disease. J Am Coll Cardiol 2023;82:1598–610.

[15] Murthy VL, Bateman TM, Beanlands RSB, Berman DS, Borges-Neto S, Chareonthaitawee P, et al. Clinical quantification of myocardial blood flow using PET: joint position paper of the SNMMI cardiovascular Council and the ASNC. J Nucl Med 2018;59:273–93.

[16] Maddahi J, Packard RRS. Cardiac PET perfusion tracers: current status and future directions. Semin Nucl Med 2014;44:333–43.

[17] David S, Packard RRS. Prevalence and nature of extracardiac findings in PET/CT myocardial perfusion imaging. J Nucl Cardiol 2023;30:1469–73.

[18] Lortie M, Beanlands RS, Yoshinaga K, Klein R, Dasilva JN, DeKemp RA. Quantification of myocardial blood flow with 82Rb dynamic PET imaging. Eur J Nucl Med Mol Imag 2007;34:1765–74.

[19] Lautamaki R, George RT, Kitagawa K, Higuchi T, Merrill J, Voicu C, et al. Rubidium-82 PET-CT for quantitative assessment of myocardial blood flow: validation in a canine model of coronary artery stenosis. Eur J Nucl Med Mol Imag 2009;36:576–86.

[20] El Fakhri G, Kardan A, Sitek A, Dorbala S, Abi-Hatem N, Lahoud Y, et al. Reproducibility and accuracy of quantitative myocardial blood flow assessment with (82)Rb PET: comparison with (13)N-ammonia PET. J Nucl Med 2009;50:1062–71.

[21] Krivokapich J, Huang SC, Phelps ME, MacDonald NS, Shine KI. Dependence of 13NH3 myocardial extraction and clearance on flow and metabolism. Am J Physiol 1982;242:H536–42.

[22] Hutchins GD, Schwaiger M, Rosenspire KC, Krivokapich J, Schelbert H, Kuhl DE. Noninvasive quantification of regional blood flow in the human heart using N-13 ammonia and dynamic positron emission tomographic imaging. J Am Coll Cardiol 1990;15:1032–42.

[23] Muzik O, Beanlands RS, Hutchins GD, Mangner TJ, Nguyen N, Schwaiger M. Validation of nitrogen-13-ammonia tracer kinetic model for quantification of myocardial blood flow using PET. J Nucl Med 1993;34:83–91.

[24] Iida H, Kanno I, Takahashi A, Miura S, Murakami M, Takahashi K, et al. Measurement of absolute myocardial blood flow with H215O and dynamic positron-emission tomography. Strategy for quantification in relation to the partial-volume effect. Circulation 1988;78:104–15.
[25] Iida H, Rhodes CG, de Silva R, Araujo LI, Bloomfield PM, Lammertsma AA, Jones T. Use of the left ventricular time-activity curve as a noninvasive input function in dynamic oxygen-15-water positron emission tomography. J Nucl Med 1992;33:1669–77.
[26] Harms HJ, Knaapen P, de Haan S, Halbmeijer R, Lammertsma AA, Lubberink M. Automatic generation of absolute myocardial blood flow images using [15O]H2O and a clinical PET/CT scanner. Eur J Nucl Med Mol Imag 2011;38:930–9.
[27] Joutsiniemi E, Saraste A, Pietila M, Maki M, Kajander S, Ukkonen H, et al. Absolute flow or myocardial flow reserve for the detection of significant coronary artery disease? Eur Heart J Cardiovasc Imaging 2014;15:659–65.
[28] Danad I, Uusitalo V, Kero T, Saraste A, Raijmakers PG, Lammertsma AA, et al. Quantitative assessment of myocardial perfusion in the detection of significant coronary artery disease: cutoff values and diagnostic accuracy of quantitative [(15)O]H2O PET imaging. J Am Coll Cardiol 2014;64:1464–75.
[29] Packard RRS. The clinical promise of (18)F-flurpiridaz PET imaging heralds a new frontier in the diagnosis and management of coronary artery disease. Nat Cardiovasc Res 2025;4:1–4.
[30] Otaki Y, Van Kriekinge SD, Wei CC, Kavanagh P, Singh A, Parekh T, et al. Improved myocardial blood flow estimation with residual activity correction and motion correction in (18)F-flurpiridaz PET myocardial perfusion imaging. Eur J Nucl Med Mol Imag 2022;49:1881–93.
[31] Poitrasson-Riviere A, Moody JB, Renaud JM, Hagio T, Arida-Moody L, Buckley C, et al. Impact of residual subtraction on myocardial blood flow and reserve estimates from rapid dynamic PET protocols. J Nucl Cardiol 2022;29:2262–70.
[32] Yalamanchili P, Wexler E, Hayes M, Yu M, Bozek J, Kagan M, et al. Mechanism of uptake and retention of F-18 BMS-747158-02 in cardiomyocytes: a novel PET myocardial imaging agent. J Nucl Cardiol 2007;14:782–8.
[33] Yu M, Guaraldi MT, Mistry M, Kagan M, McDonald JL, Drew K, et al. BMS-747158-02: a novel PET myocardial perfusion imaging agent. J Nucl Cardiol 2007;14:789–98.
[34] Huisman MC, Higuchi T, Reder S, Nekolla SG, Poethko T, Wester HJ, et al. Initial characterization of an 18F-labeled myocardial perfusion tracer. J Nucl Med 2008;49:630–6.
[35] Nekolla SG, Reder S, Saraste A, Higuchi T, Dzewas G, Preissel A, et al. Evaluation of the novel myocardial perfusion positron-emission tomography tracer 18F-BMS-747158-02: comparison to 13N-ammonia and validation with microspheres in a pig model. Circulation 2009;119:2333–42.
[36] Sherif HM, Saraste A, Weidl E, Weber AW, Higuchi T, Reder S, et al. Evaluation of a novel (18)F-labeled positron-emission tomography perfusion tracer for the assessment of myocardial infarct size in rats. Circ Cardiovasc Imaging 2009;2:77–84.
[37] Yu M, Nekolla SG, Schwaiger M, Robinson SP. The next generation of cardiac positron emission tomography imaging agents: discovery of flurpiridaz F-18 for detection of coronary disease. Semin Nucl Med 2011;41:305–13.
[38] Sherif HM, Nekolla SG, Saraste A, Reder S, Yu M, Robinson S, et al. Simplified quantification of myocardial flow reserve with flurpiridaz F 18: validation with microspheres in a pig model. J Nucl Med 2011;52:617–24.
[39] Guehl NJ, Normandin MD, Wooten DW, Rozen G, Sitek A, Ruskin J, et al. Single-scan rest/stress imaging: validation in a porcine model with (18)F-Flurpiridaz. Eur J Nucl Med Mol Imag 2017;44:1538–46.
[40] Renaud JM, Poitrasson-Riviere A, Moody JB, Hagio T, Ficaro EP, Murthy VL. Improved diagnostic accuracy for coronary artery disease detection with quantitative 3D (82)Rb PET myocardial perfusion imaging. Eur J Nucl Med Mol Imag 2023;51:147–58.
[41] Slomka PJ, Nishina H, Berman DS, Akincioglu C, Abidov A, Friedman JD, et al. Automated quantification of myocardial perfusion SPECT using simplified normal limits. J Nucl Cardiol 2005;12:66–77.
[42] Packard RRS, Cooke CD, Van Train KF, Votaw JR, Sayre JW, Lazewatsky JL, et al. Development, diagnostic performance, and interobserver agreement of a (18)F-flurpiridaz PET automated perfusion quantitation system. J Nucl Cardiol 2022;29:698–708.
[43] Moody JB, Poitrasson-Riviere A, Hagio T, Buckley C, Weinberg RL, Corbett JR, et al. Added value of myocardial blood flow using (18)F-flurpiridaz PET to diagnose coronary artery disease: the flurpiridaz 301 trial. J Nucl Cardiol 2021;28:2313–29.
[44] Ficaro EP, Lee BC, Kritzman JN, Corbett JR. Corridor4DM: the Michigan method for quantitative nuclear cardiology. J Nucl Cardiol 2007;14:455–65.
[45] Slomka PJ, Rubeaux M, Le Meunier L, Dey D, Lazewatsky JL, Pan T, et al. Dual-gated motion-frozen cardiac PET with flurpiridaz F 18. J Nucl Med 2015;56:1876–81.
[46] Packard RRS, Huang SC, Dahlbom M, Czernin J, Maddahi J. Absolute quantitation of myocardial blood flow in human subjects with or without myocardial ischemia using dynamic flurpiridaz F 18 PET. J Nucl Med 2014;55:1438–44.
[47] Packard RRS, Votaw JR, Cooke CD, Van Train KF, Garcia EV, Maddahi J. 18F-flurpiridaz positron emission tomography segmental and territory myocardial blood flow metrics: incremental value beyond perfusion for coronary artery disease categorization. Eur Heart J Cardiovasc Imaging 2022;23:1636–44.
[48] Builoff V, Huang C, Kuronuma K, Wei CC, Fujito H, Otaki Y, et al. Automatic motion correction for myocardial blood flow estimation improves diagnostic performance for coronary artery disease in (18)F-flurpiridaz positron emission tomography-myocardial perfusion imaging. J Nucl Cardiol 2024:102072.
[49] Tsukada H, Nishiyama S, Fukumoto D, Kanazawa M, Harada N. Novel PET probes 18F-BCPP-EF and 18F-BCPP-BF for mitochondrial complex I: a PET study in comparison with 18F-BMS-747158-02 in rat brain. J Nucl Med 2014;55:473–80.
[50] Rosenspire KC, Schwaiger M, Mangner TJ, Hutchins GD, Sutorik A, Kuhl DE. Metabolic fate of [13N]ammonia in human and canine blood. J Nucl Med 1990;31:163–7.
[51] Bormans G, Maes A, Langendries W, Nuyts J, Vrolix M, Vanhaecke J, et al. Metabolism of nitrogen-13 labelled ammonia in different conditions in dogs, human volunteers and transplant patients. Eur J Nucl Med 1995;22:116–21.
[52] Zunkeler B, Carson RE, Olson J, Blasberg RG, Girton M, Bacher J, et al. Hyperosmolar blood-brain barrier disruption in baboons: an in vivo study using positron emission tomography and rubidium-82. J Neurosurg 1996;84:494–502.
[53] Levin CS, Hoffman EJ. Calculation of positron range and its effect on the fundamental limit of positron emission tomography system spatial resolution. Phys Med Biol 1999;44:781–99.
[54] Johnson NP, Sdringola S, Gould KL. Partial volume correction incorporating Rb-82 positron range for quantitative myocardial perfusion PET based on systolic-diastolic activity ratios and phantom measurements. J Nucl Cardiol 2011;18:247–58.